Chinese Chemical Letters 32 (2021) 3596–3600

Contents lists available at ScienceDirect

Chinese Chemical Letters

journal homepage: www.elsevier.com/locate/cclet

Communication

Facile preparation of hydrogenated graphene by hydrothermal methods and the investigation of its ferromagnetism

Yunpeng Wu, Yi Feng, Zhongyu He, Deyang Yu, Ying Xue, Xilong Liu, Leiyun Han, Xudong Zhao*, Xiaoyang Liu*

State Key Laboratory of Inorganic Synthesis and Preparative Chemistry, College of Chemistry, Jilin University, Changchun 130012, China

ARTICLE INFO

Article history:
Received 15 January 2021
Received in revised form 18 February 2021
Accepted 23 March 2021
Available online 26 March 2021

Keywords:
Graphene
Hydrogenation
Hydrothermal method
Ferromagnetism
Carbon materials

ABSTRACT

In this paper, a hydrothermal approach is utilized for the first time in integrating graphene oxide (GO), acetic acid (HAc) and nickel foam to prepare hydrogenated graphene (HG). There are two primary aims of this study: one is to ascertain the structure of the as-prepared HG, and the other one is to investigate the ferromagnetism of the HG. Under hydrothermal conditions, GO was reduced and hydrogenated by HAc, while the nickel foam served as a catalyst. This work provides a novel and facile route for the synthesis of hydrogenated graphene, which may lead to the application of hydrogenated graphene in spin electronic devices.

Nanomaterials with magnetism are of great interest because they play a critical role in current technological applications [1]. However, to the best of our knowledge, most magnetic nanomaterials contain *d* and *f* elements that can be harmful to the environment [2]. Therefore, there is an urgent need for non-metallic magnetic materials that can be used in industrial applications. In recent years, there has been an increasing interest regarding the ferromagnetism of carbon-based materials [3–6]. A considerable amount of literature has been published around the theme of ferromagnetism of highly oriented pyrolytic graphite (HOPG) [7,8], room-temperature ferromagnetic carbon nanotubes [9,10] and soft magnetic C_{60} [11,12].

Another key aspect of carbon-based materials is graphene, which has many outstanding properties such as large specific area, high conductivity, and excellent stability [13–15]. However, the main challenge faced by many researchers is that graphene suffers from a zero band gap that makes graphene non-magnetic [16]. Therefore, inducing magnetism to graphene is a major area of interest within the field of magnetic nanomaterials. Research has shown that ferromagnetism can be effectively induced in graphene by heteroatom doping, creating defects, or creating composites with other materials [5,17–20].

Among the wide range of graphene derivatives, hydrogenated graphene has been an object of research since 2003 when Sluiter predicted the atomic structure of hydrogenated graphene [21]. Many theoretical and experimental studies have been performed since to explore the properties and potential applications of hydrogenated graphene, including energy storage [22], catalytic performance [23] and magnetism [24]. Later, the ferromagnetism of semi-hydrogenated graphene sheets was predicted by Zhou using density functional theory [24]. Data from this study suggested that semi-hydrogenated graphene will become a ferromagnetic semiconductor with a small indirect gap. In the semi-hydrogenated graphene hexagonal framework, valence electrons in p-states are delocalized so that they can have more spatial extension that can promote long-range magnetic coupling interactions. This gives rise to an infinite magnetic sheet with structural integrity and magnetic homogeneity, making hydrogenated graphene very appealing for further experiments [25].

Graphene is a nearly perfect two-dimensional system and chemically inert [1,13]. Therefore, the formation of carbon-hydrogen bonds in graphene requires an aggressive reaction condition. According to a previous review, the preparation method can be categorized into four prominent routes: Plasma hydrogenation, thermal cracking, dissolving metal reduction and electrochemical hydrogenation [26,27]. Of these, thermal cracking can thermally generate atomic hydrogen applied to graphene; this method is usually safe and clean [28]. Poh presented a scalable method for the hydrogenation of graphene under the condition of 100 bar and 500 °C from GO. The content of hydrogen was detected to be 11.6% by combustion elemental analysis [29]. Antonov synthesized multilayer hydrogenated graphene at pressures above

* Corresponding authors.
E-mail addresses: xdzhao@jlu.edu.cn (X. Zhao), liuxy@jlu.edu.cn (X. Liu).

https://doi.org/10.1016/j.cclet.2021.03.062

2 GPa and temperatures from 450 °C to 700 °C inside high-pressure cells. The atomic ratio of H/C was calculated by X-ray diffraction to be 0.94 [30]. Previous research showed that thermal cracking has great potential to serve as a facile pathway towards the mass production of hydrogenated graphene. However, little attention has been given to hydrothermal methods to prepare hydrogenated graphene.

Here, we present a facile hydrothermal method to prepare hydrogenated graphene from GO and HAc using a nickel foam catalyst. Through hydrogenation, the original sp^2 structure of graphene will be destroyed, and the surface will produce sp^3-C—H bonds [31–33]. The as-prepared sample will be characterized by X-ray diffraction, Raman spectroscopy, scanning electron microscopy, transmission electron microscopy, X-ray photoelectron spectroscopy and infrared spectroscopy. Furthermore, the magnetism of the as-prepared samples was analyzed by a superconducting quantum interference device. This work offers fresh insight into the preparation of hydrogenated graphene and contributes to a deeper understanding of the ferromagnetism of hydrogenated graphene.

The process of preparing hydrogenated graphene is shown in Scheme 1. A commercially purchased GO aqueous solution (10 mL, 1 mg/mL) was mixed with 10 mL HAc (analytically pure) in a centrifuge tube. After ultrasonic dispersion for 15 min, the mixture was poured into a Teflon-lined stainless-steel autoclave with a piece of nickel foam (2 × 3 cm, 0.19 ± 0.01 g). The autoclave was heated in an electric oven for 12 h at various temperatures (100 °C, 120 °C, 140 °C, 160 °C or 180 °C) and naturally cooled to room temperature. The as-prepared sample without nickel foam was repeatedly washed with hydrochloric acid (analytically pure) to remove residual nickel particles. The sample was then washed with deionized water until the pH reached 7 to remove residual H^+. Finally, the samples were put into a vacuum drying chamber at 80 °C. The samples reacted under different temperatures were defined as HG-100, HG-120, HG-140, HG-160 and HG-180.

Field-emission scanning electron microscopy (SEM, JEOL JSM 6700 F) and transmission electron microscopy (TEM, FEI Tecnai G2 F20 S-Twin D573) with an acceleration voltage of 200 kV were utilized to characterize the morphology of the samples. X-ray diffraction (XRD, Rigaku D/Max 2550 V/PC, Japan Cu-Kα radiation, λ =0.15418 nm) and Raman microscopy (Renishaw inVia Confocal Raman spectrometer using a solid-state laser at 532 nm as the excitation source) wereused to examine and analyze the composition and structure of the samples. The binding information and surface chemical compositions were examined by X-ray photoelectron spectroscopy (XPS, Thermo ESCALab 250) and Fourier-transform infrared spectroscopy (FTIR, Thermo ESCALAB250).

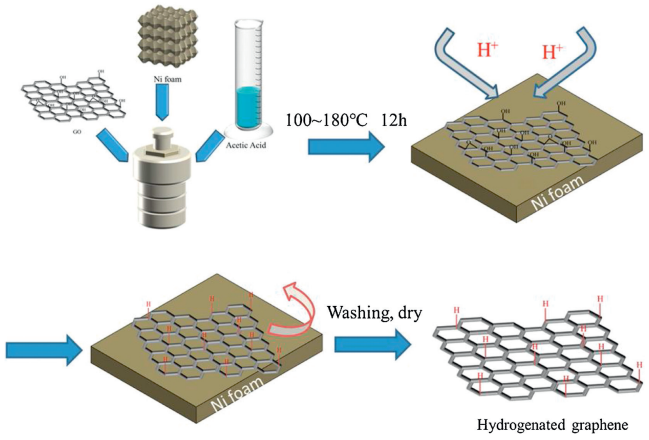

Scheme 1. Process of preparing hydrogenated graphene.

Inductively-coupled plasma optical emission spectrometry (ICP, iCAP 7600 ICP-OES) was used to measure the ferromagnetic impurities. The ferromagnetism of the samples was measured on a superconducting quantum interference device (SQUID, Quantum Design Inc.).

First, the morphology of the sample was characterized by SEM and TEM. Figs. 1a and b show SEM images of HG-160 at low resolution and high resolution, respectively. The results revealed that the sample has multiple layers with many wrinkles. The wrinkle is a characteristic feature of single-layer graphene, which proves that the content of HG-160 in a monolayer structure predominates. Figs. 1c and d show TEM images of HG-160. The TEM images of HG-160 in Figs. 1c and d also confirmed that the sample have a layer-structure. The large size of the hydrogenated graphene (more than 1 μm) gives the material wider potential application prospects. Figs. 1e and f show the SEM and TEM images of HG-100. Compared with HG-160, it shows less wrinkles which indicated that there is reduced monolayer structure within the sample.

X-ray diffraction (XRD) was used to investigate the structure of the samples. All samples had a wide peak around $2\theta = 21°$ that corresponded to the (002) lattice plane of graphene; some of the samples had a weak peak around $2\theta = 44°$ that corresponded to the (111) lattice plane of graphene (Fig. 2a). The position of the (002) lattice plane was different from normal graphite or graphene that should appear at $2\theta = 26.3°$. The reason for this phenomenon is that the samples prepared from GO by a hydrothermal method are reduced graphene oxide (RGO), whose (002) characteristic peak should appear around $2\theta = 20°$ [13]. Another important finding was that from HG-100 to HG-160, the peak at $2\theta = 21°$ broadens. A possible explanation for this might be the reduction of GO accompanied by hydrogenation.

Our previous research has shown that controllable hydrogenation of graphene can be obtained by high energy ball-milling methods with acetic acid as the hydrogenating agent [34]. Hydrogen atoms break the integrity of the sp^2 structure and give the graphene a higher density of defects. In the hydrogenated process, nickel foam also plays a critical role in the catalyst. Skeletal nickel is normally used for catalyzing the hydrogenation of

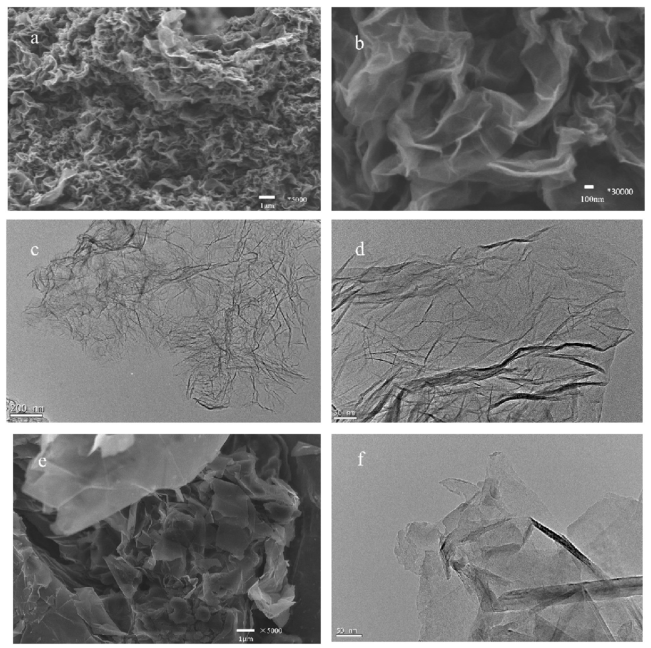

Fig. 1. (a, b) SEM images HG-160. (c, d) TEM images of HG-160. (e, f) SEM and TEM images of HG-100.

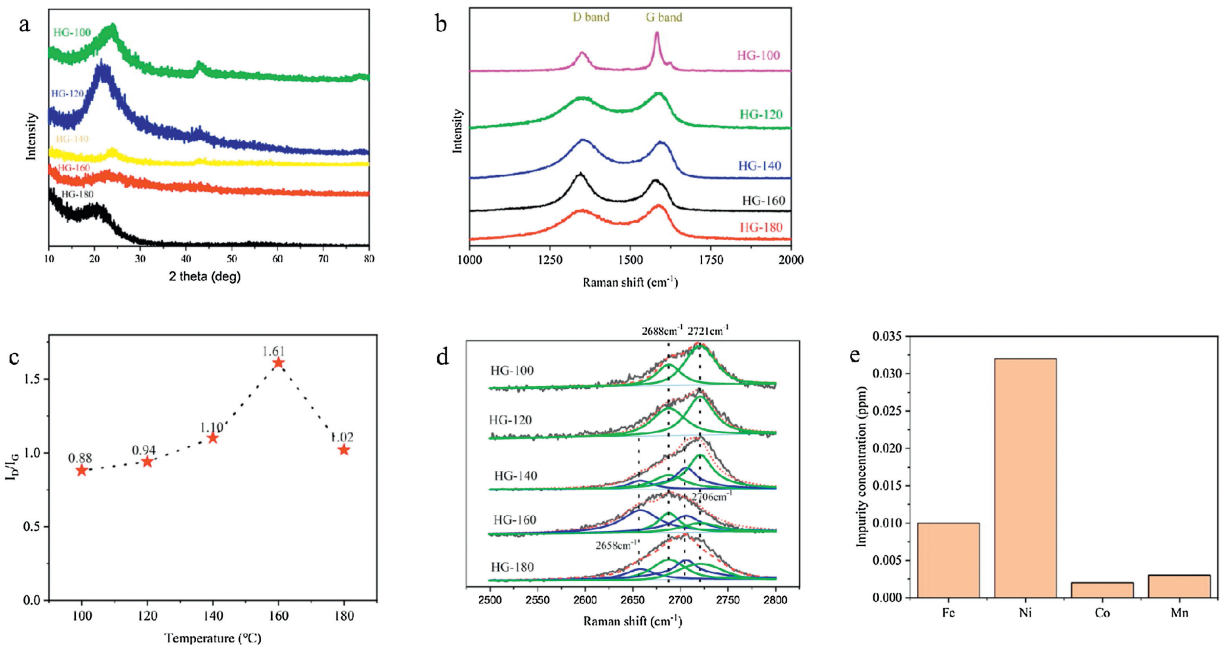

Fig. 2. (a) XRD results of the samples. (b, c) Raman results and I_D/I_G values of the samples. (d) The measured 2D Raman band of the samples. (e) Contents of the metal impurities (such as Fe, Ni, Co or Mn) of HG-160 measured *via* ICP-OES.

benzene. Inspired by this idea, Zheng used nickel to catalyze the hydrogenation of graphene films [35]. Nickel foam has a high specific area with porous structure, which allows for catalytically active sites than normal nickel particles. It is also stable such that it cannot be dissolved by HAc. Therefore, nickel foam is an excellent candidate for catalyzing the hydrogenation of graphene. In HG-180, the peak near $2\theta = 21^\circ$ was sharper than that of HG-160. This result may be because the C—H is not stable at high temperature. Conventionally, C—H is recognized as being highly stable, but it will completely decompose when at a temperature of 1200 K. However, based on Smith's earlier observations, the C—H bond strength in the carbon skeleton of graphene is much weaker than normal C—H bonds [36]. This finding is consistent with our results that the C—H is not stable at 180 °C, and causes the HG-180 have a sharper peak near $2\theta = 21^\circ$.

The evolution of the Raman spectra of hydrogenated graphene was measured at different temperatures (Fig. 2b). Prior studies have noted that the sp^2 graphene lattice (G peak, 1580 cm^{-1}) as well as related defects in the sp^2 lattice (D peak, 1350 cm^{-1}) can be identified by Raman spectroscopy [25]. The intensity ratio of the D peak and the G peak (I_D/I_G) is an index for measuring the density of defects in graphene. As mentioned in the literature review, a benchmark of $I_D/I_G = 2$ is equivalent to ~10% atomic coverage of hydrogen [33]. From 100 °C to 160 °C, the I_D/I_G value generally increased with temperature (Fig. 2c). However, the I_D/I_G value of HG-180 is smaller than HG-160. This tendency is consistent with that of the XRD results and confirms our previous explanation. HG-160 showed the highest I_D/I_G value at 1.61. Although this value does not reach the benchmark of 2, it still confirmed that HG-160 has a high density of defects due to the hydrogenation process. In Fig. 2d, we present the Gaussian fitting 2D Raman band of the samples. As can be seen in HG-140, HG-160 and HG-180, the 2D band can be fitted to 4 peaks, located at 2658 cm^{-1}, 2688 cm^{-1}, 2706 cm^{-1} and 2721 cm^{-1} respectively, which were consistent with the reported results from L.M. Malard about Raman spectra for few-layer graphene [37]. In his study, he demonstrated that the 2D band of the sample that has higher intensity of the low-frequency Gaussian fitting peak tends to have fewer layers. According to the observation of Gaussian fitting peak intensity in the samples, the number of layers of HG-160 was the fewest. When the number of layers is more than 6, the Raman peak of graphene coincides with the Raman peak of graphite, fitting two peaks at 2688 cm^{-1} and 2721 cm^{-1}, and therefore the HG-100 and HG-120 is more than 6 layers [37]. ICP is an invaluable instrument to carefully check the content of the ferromagnetic impurities in all our samples. In Fig. 2e, the results of ICP showed that only less than 0.05 ppm of the ferromagnetic impurities (Fe, Ni, Co and Mn) could be detected. This result indicated that the content of ferromagnetic impurities is negligible, and the contribution of magnetic impurities can be ignored.

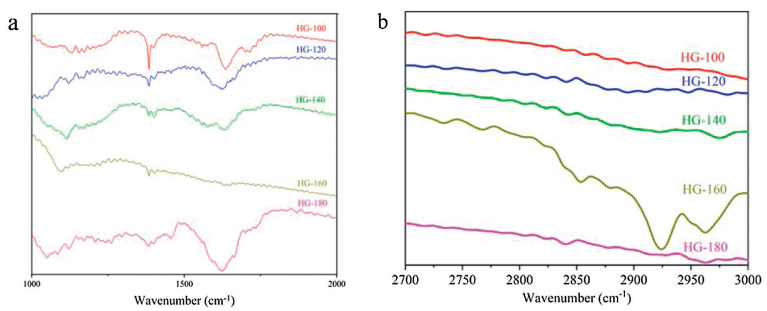

Fig. 3. (a, b) FT-IR results of samples in high and low wavenumber, respectively.

FT-IR is a characterization technique used to study C—H bonds. In Figs. 3a and b, we showed the FT-IR results of the samples. According to previous research, the wavenumber at 1370 cm^{-1} represents the C—OH bending and the skeletal vibration of graphene is located around 1600–1650 cm^{-1} [22]. The data in Fig. 3a showed that the skeletal vibration has a high intensity in HG-100. However, from HG-100 to HG-160, there is a clear decreasing trend. The observed decrease in graphene skeletal vibration could be attributed to the increasing density of defects induced by hydrogen atoms. However, the intensity of the graphene skeletal vibration in HG-180 is much higher than that of HG-160. It is likely that this result was due to the C—H bonds in HG-180 being unstable and thus dehydrogenated to HGO at this temperature. The intensity of C—OH bending shows a decreasing trend because of the reduction of GO. Interestingly, the vibration band from C=O groups in carboxylic acid (1700–1750 cm^{-1}) was not present in the results, which indicated that —COOH is not absorbed on the surface of samples and will not contribute to the ferromagnetism of the samples. The C—H vibration band is located near 2900 cm^{-1} and only in the FT-IR of HG-160; this band is conspicuous, which indicates a high degree of hydrogenation in HG-160.

XPS is an effective tool to infer the level of hydrogenation by analyzing the C 1s signal while providing detailed information on the chemical composition of the samples. Typically, the C 1s peak can be fitted to the C=C bond at 284.4 eV, the C—C—H bond at 285.5 eV, the C—O bond at 286.5 eV, and the C=O bond at 288.0 eV [22]. As shown in Fig. 4a, the intensity of the C—O bond and the C=O bond decreased significantly, indicating that GO was reduced by HAc under the condition of high temperature. The intensities obtained from the C 1s deconvolution can also be used as indirect proof of the presence of the C—H bond. As seen from Fig. 4b, HG-160 had the highest proportion of C—C—H (C—C—H /C=C = 1.23). The result of the C—C—H /C=C value is consistent with the Raman spectroscopy data. From 100 °C to 160 °C, the C—C—H /C=C value increased with temperature. However, the C—C—H /C=C value of HG-180 is smaller than HG-160. According to these results, we infer that the degree of hydrogenation increases from 100 °C to 160 °C. However, as the temperature continues to rise past these temperatures, the C—H bonds will be unstable, thus leading to dehydrogenation. Fig. 4c shows the wide-range of XPS spectra for HG-160, and it was found that only carbon elements and a small amount of oxygen are present in HG-160.

SQUID was employed to measure the magnetic properties of the samples. Figs. 5a and b are the hysteresis loops of HG-100, HG-120, HG-140, HG-160 and HG-180, respectively, measured at 2 K. These results are quite revealing in several ways. First, the hysteresis loops of HG-100, HG-120, and HG-140 (Fig. 5a) show paramagnetic characteristics that are consistent with Tang's work, where the GO is spin 5/2 paramagnetic and the origin of the localized magnetic moments is from hydroxyl groups that are abundant in HG-100, HG-120 and HG-140 [38]. Second, HG-160 and HG-180 showed typical ferromagnetic hysteresis loops (Fig. 5b), which means that paramagnetism transforms into ferromagnetism at 160 °C. The ferromagnetism of HG-160 mainly originated from the induction of the hydrogen atoms that can break the delocalized π bonding network and make the electrons more unpaired than that in normal graphene. The ferromagnetism caused by hydrogenation is very different from that caused by defects. That is because hydrogenation results in long range magnetic ordering in graphene and give rise to the integrated ferromagnetism of graphene structure rather than a heterogenous magnetism. The effect of this structural integrated ferromagnetism is stronger than that of localized magnetism and thus the ferromagnetism is mainly caused by hydrogenation [24,39]. Furthermore, HG-160 is mainly in a single-layer structure, which makes its electronic structure tend to have metal-semiconductor properties and thus makes its ferromagnetism more pronounced [24,40]. The saturation magnetic moment (M_S) of HG-160 is 0.029 emu/g, which is higher than that of HG-180 (0.019 emu/g). A possible explanation for this result is that the magnetic moments from the hydrogen atoms give rise to a magnetic sheet with structural integrity and magnetic homogeneity. This theory is different from traditional ferromagnetic studies of graphene whereby defects are created from zigzag edges [24]. The structural integrity and magnetic homogeneity help the graphene promote long-range magnetic coupling interactions. Therefore, hydrogenated graphene shows stronger ferromagnetism than defective graphene with zigzag edges. The C—H bonds are dehydrogenated in HG-180, making HG-180 become RGO. The ferromagnetism of HG-180 originated from zigzag edges that were created by the high density of defects. Thus, HG-160 shows higher M_S than HG-180. Finally, the hysteresis loops of HG-160 measured

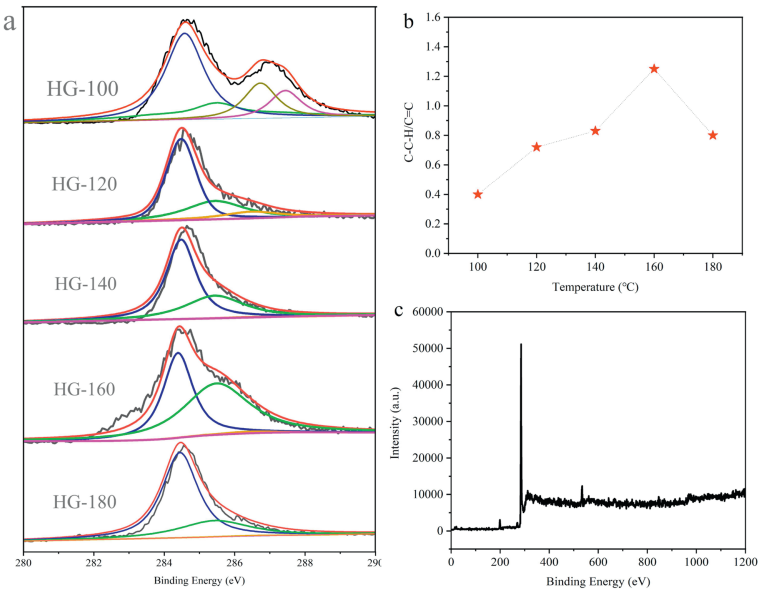

Fig. 4. (a) High-resolution C 1s peak of HG-100, HG-120, HG-140, HG-160 and HG-180. (b) C-C-H/C=C value of the samples. (c) Wide-range XPS spectra of HG-160.

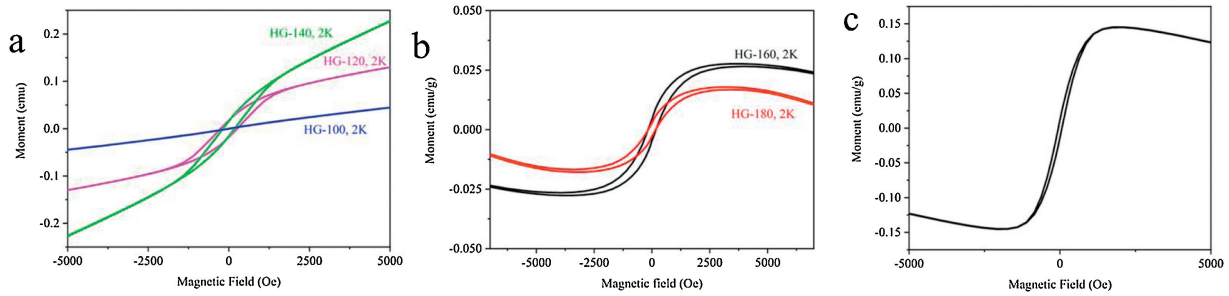

Fig. 5. (a) MT curves of HG-100, HG-120 and HG-140 at 2 K. (b) MT curves of HG-160 and HG-180 at 2 K. (c) MT curve of HG-160 at 300 K.

at 300 K are shown on Fig. 5c. The observed ferromagnetic saturation moment in HG-160 at 300 K is 0.015 emu/g, indicating that the HG-160 also has ferromagnetism in room temperature. This finding is consistent with that of Eng who found evidence of room-temperature ferromagnetism in hydrogenated graphene oxide [41].

Compared with other hydrogenation methods, such as those of Zhao (0.015 emu/g at 5 K and 0.013 emu/g at 300 K) [42], Eng (0.006 emu/g at both 5 K and 300 K) [41] and Sun (0.274 A m^2/kg at 2 K) [34], our hydrothermal method is simpler and more convenient, and the hydrogenated graphene also has certain ferromagnetism in both room temperature (0.015 emu/g) and low temperature condition (0.029, 2 K).

In conclusion, this study explored a facile hydrothermal method to prepare the hydrogenated graphene and evaluate its ferromagnetism. The as-prepared samples were exhaustively characterized, and the results showed that GO was reduced and hydrogenated by HAc. The evidence suggests that the sample has a high degree of hydrogenation, and the value of C—C—H/C=C is 1.23 and I_D/I_G is 1.61. The magnetism of the samples was also tested by SQUID. These data suggest that ferromagnetism can be achieved through the hydrogenation of graphene, and a high ferromagnetic saturation moment is seen. These findings can provide insights into ferromagnetic graphene for future research.

Declaration of competing interest

The authors report no declarations of interest.

Acknowledgments

This work was supported by National Natural Science Foundation of China (Nos. 21271082 and 21371068).

References

[1] L. Zong, X. Chen, S. Dou, et al., Chin. Chem. Lett. 32 (2021) 1121-1126..
[2] Q. Zeng, Z. Lei, J. Yang, et al., IOP Conf. Ser.: Earth Environ. Sci. 513 (2020) 012001.
[3] S. Guo, F. Zhang, D. Li, et al., J. Mol. Struct. 1221 (2020) 128887.
[4] Y. Zhang, S. Talapatra, S. Kar, et al., Phys. Rev. Lett. 99 (2007) 107201.
[5] Z.J. Yue, D.H. Seo, K. Ostrikov, et al., Appl. Phys. Lett. 104 (2014) 092417.
[6] Y. Wu, Q. Sun, D. Yu, et al., Chem. Eng. Sci. 233 (2021) 116395.
[7] M. Sepioni, R.R. Nair, I.L. Tsai, et al., EPL 97 (2012) 47001.
[8] H. Xia, W. Li, Y. Song, et al., Adv. Mater. 20 (2008) 4679–4683.
[9] A.N. Zakhlevnykh, D.A. Petrov, P.K. Skokov, J. Exp, Theor. Phys. 127 (2018) 767–777.
[10] X. Wang, F. Sharif, X. Liu, et al., J. CO_2 Util. 40 (2020) 101218.
[11] D. Zhou, F. Han, L. Ding, et al., J. Chromatogra. B 1144 (2020) 122076.
[12] X. Shao, L. Li, X. Shi, et al., Nanoscale 11 (2019) 6228–6234.
[13] Y. Zhu, S. Murali, W. Cai, et al., Adv. Mater. 22 (2010) 3906–3924.
[14] S. Liu, P. Wang, C. Liu, et al., Small 16 (2020) 2002856.
[15] Y. Wu, X. Liu, D. Xia, et al., Chin. Chem. Lett. 31 (2020) 559–564.
[16] E.W. Hill, A.K. Geim, K. Novoselov, et al., J. Am. Chem. Soc. 139 (2017) 3171–3180.
[17] Y. Liu, Y. Shen, L. Sun, et al., Nat. Commun. 7 (2016) 10921.
[18] Q. Miao, L. Wang, Z. Liu, et al., Sci. Rep. 6 (2016) 21832.
[19] Y. Wu, Q. Sun, D. Yu, et al., Chem. Commun. 56 (2020) 2016–2019.
[20] M. Sluiter, Y. Kawazoe, et al., Phys. Rev. B 43 (2003) 338–344.
[21] Z. Sofer, O. Jankovský, P. Šimek, et al., Nanoscale 6 (2014) 2153–2160.
[22] X. Han, X. Tong, X. Liu, et al., ACS Catal. 8 (2018) 1828–1836.
[23] J. Zhou, Q. Wang, Q. Sun, et al., Nano Lett. 9 (2009) 3867–3870.
[24] M.S. Dresselhaus, A. Jorio, M. Hofmann, et al., Nano Lett. 10 (2010) 751–758.
[25] M. Pumera, C.H.A. Wong, et al., Chem. Soc. Rev. 42 (2013) 5987–5995.
[26] K.E. Whitener, et al., J. Vac. Sci. Technol. A 36 (2018) 05G401.
[27] S. Dou, J. Xu, X. Cui, et al., Adv. Energy Mater. 10 (2020) 2001331.
[28] H.L. Poh, F. Šaněk, Z. Sofer, M. Pumera, et al., Nanoscale 4 (2012) 7006–7011.
[29] V.E. Antonov, I.O. Bashkin, A.V. Bazhenov, et al., Carbon 100 (2016) 465–473.
[30] L. Xie, X. Wang, J. Lu, et al., Appl. Phys. Lett. 98 (2011) 193113.
[31] V.M. Mikoushkin, S.Y. Nikonov, A.T. Dideykin, et al., Appl. Phys. Lett. 102 (2013) 071910.
[32] Y. Fei, S. Fang, Y.H. Hu, et al., Chem. Eng. J. 397 (2020) 125408.
[33] Q. Sun, X. Wang, B. Li, et al., Chem. Res. Chinese U. 34 (2018) 344–349.
[34] L. Zheng, Z. Li, S. Bourdo, et al., Chem. Commun. 47 (2011) 1213–1215.
[35] D. Smith, R.T. Howie, I.F. Crowe, et al., ACS Nano 9 (2015) 8279–8283.
[36] L.M. Malard, M.A. Pimenta, G. Dresselhaus, M.S. Dresselhaus, et al., Phys. Rep. 473 (2009) 51–87.
[37] T. Tang, F. Liu, Y. Liu, et al., Appl. Phys. Lett. 104 (2014) 123104.
[38] S. Li, L. Tian, L. Shi, et al., J. Phys-Condens. Matt. 28 (2016) 086001.
[39] E. Vishnyakova, G. Chen, B.E. Brinson, et al., Accounts Chem. Res. 50 (2017) 1351–1358.
[40] A.Y.S. Eng, H.L. Poh, F. Šaněk, et al., ACS Nano 7 (2013) 5930–5939.
[41] M. Zhao, H. Xiao, S. Chen, et al., RSC Adv. 8 (2018) 13148–13153.